Effects of Axial Flux Magnetic Gear Misalignment

Bryton Praslicka
Dept. of Elec. And Comp. Engr.
Texas A&M University
College Station, Texas 77843
bryton.praslicka@tamu.edu

Matthew Johnson
Army Research Lab
U. S. Army CCDC
College Station, TX, USA
matthew.c.johnson186.civ@mail.mil

Matthew C. Gardner
Dept. of Elec. And Comp. Engr.
Texas A&M University
College Station, Texas 77843
gardner1100@tamu.edu

Ellen Dangtran
Dept. of Elec. And Comp. Engr.
Texas A&M University
College Station, Texas 77843
ellen.dangtran@gmail.com

Hamid A. Toliyat
Dept. of Elec. And Comp. Engr.
Texas A&M University
College Station, Texas 77843
toliyat@tamu.edu

***Abstract*— Magnetic gears have recently received significant interest as a potential replacement for mechanical gears. Some papers have proposed that magnetic gears may be more tolerant to misalignment than their mechanical counterparts. This paper describes a parametric finite element analysis (FEA) study of the effects of misalignment in an axial flux magnetic gear (AFMG). A base design is selected and important parameters, including gear ratio, pole count, and outer radius, are varied to illustrate the effect of misalignment on different designs using simulation results. The torque signature of the gear tends to be more sensitive to misalignment on the high pole count rotor than on the low pole count rotor, and increasing the pole counts makes the gear more sensitive to misalignment. However, other parameters, such as magnet thicknesses, have much smaller impacts on the gear's sensitivity to misalignment. Experimental results confirm the simulated trends for the slip torque.**

Keywords—axial flux, finite element analysis, magnetic gear, misalignment, slip torque, torque ripple, wind turbine gearbox

I. INTRODUCTION

Since its inception in the 1990s, the utility-scale wind industry has suffered from unacceptably high gearbox failure rates [1]. Most modern wind turbine gearboxes, despite adherence to an internationally recognized design standard, IEC 61400-4, fail to meet their designed mean time to failure (MTTF) goal of 20 years, with most gearbox systems requiring significant repair or replacement in just 7-11 years [2]-[4]. Today, the failure of wind turbine gearboxes significantly increases the cost of wind energy because gearboxes have the longest mean time to repair (MTTR) out of the various wind turbine systems, resulting in 5 days downtime on average for turbine systems rated for 2 MW and below [5]. Despite the costly risk associated with gearbox failure outside of warranty [3] and high O&M costs of geared onshore and offshore wind projects [5]-[6], drivetrains with a three-stage planetary/helical gearbox and a high-speed asynchronous generator dominate the global market for both onshore and offshore wind projects [6] because geared drivetrains are generally cheaper and lighter than direct-drive systems [7]. The widespread use of gearboxes in wind turbines has created a reliability problem so severe that an entire market for gearbox repair has emerged [8], and the National Renewable Energy Laboratory (NREL) created a gearbox reliability collaborative to target the issue [2], [5]. In 2015, a survey of over 750 failures for wind turbine gearbox systems observed that bearing failure constitutes 76% of gearbox failures, and the gears themselves, especially the helical gear, constituted 17% of the failures [5], [9]. In 2018, NREL asserted that wind turbine gearboxes are still the most costly subsystem to maintain over a turbine's 20-year design lifetime [10]. According to NREL, these gearbox failure modes are not caused by manufacturing practices [11]. Rather, during operation, dynamic structural loading during major transient events [12] and momentary misalignment caused by uneven loading stemming from stochastic gusts of wind [3], [13] both create stress on the gears and bearings, leading to wear that results in gear or bearing failure modes such as micropitting, scuffing, or bending fatigue.

Recently, magnetic gears have received significant interest as a possible replacement for their mechanical counterparts [14]. Like mechanical gears, magnetic gears convert energy between low-speed, high-torque rotation and high-speed, low-torque rotation. However, unlike mechanical gears, magnetic gears transfer power through modulated magnetic fields, instead of direct contact between mechanical teeth. This contactless operation offers numerous potential advantages, such as reduced maintenance, improved reliability, inherent overload protection, decreased acoustic noise, and physical isolation between shafts. One paper suggested that another potential benefit of magnetic gears over mechanical gears in wind turbine applications may be increased tolerance of misalignment [15]. These potential benefits have generated significant interest in magnetic gears for wind turbines drivetrains [15]-[17], and the development of prototypes for wind turbine drivetrain applications [18]-[20]. Magnetic gear prototypes have also been developed for a plethora of other applications, including electric aircraft [21], electric vehicles [22], hybrid electric vehicle power split devices [23], and wave energy conversion [24].

While much of the existing literature focuses on variations of the coaxial radial flux magnetic gear shown in Fig. 1(a) [14]-[17], [19]-[24], the coaxial axial flux magnetic gear, shown in Fig. 1(b), also exhibits significant promise for certain design requirements [25]-[27]. The coaxial radial flux and axial flux magnetic gear (AFMG) topologies both consist of three rotors: a low pole count permanent magnet (PM) rotor (Rotor 1), a high pole count PM rotor (Rotor 3), and a modulator rotor

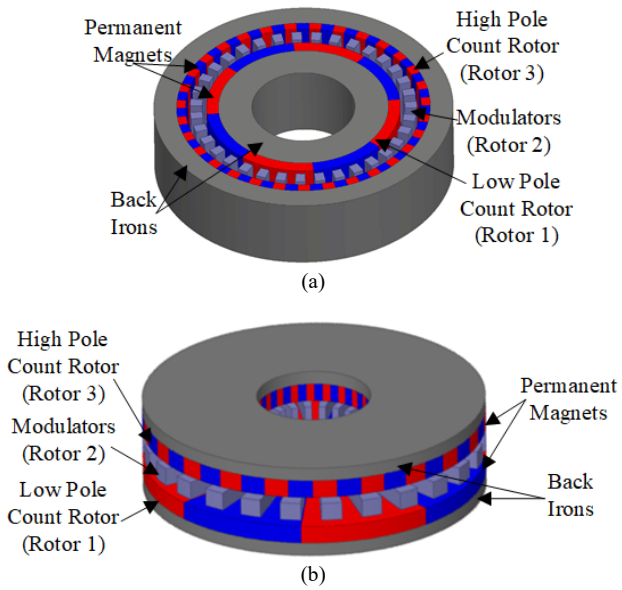

Fig. 1. Coaxial (a) radial flux and (b) axial flux magnetic gears with surface-mounted permanent magnets.

(Rotor 2). For both topologies, the relationship between the number of PM pole pairs and the modulator count is given by

$$Q_2 = P_1 + P_3, \tag{1}$$

where P_1 is the number of pole pairs on Rotor 1, P_3 is the number of pole pairs on Rotor 3, and Q_2 is the number of modulators. If the modulators are fixed, Rotor 1 and Rotor 3 operate as the high and low speed rotors, respectively, and their steady-state speeds are related by the gear ratio defined by

$$\text{Gear Ratio} = \frac{\omega_1}{\omega_3} = \frac{-P_3}{P_1}, \tag{2}$$

where ω_1 and ω_3 are the speeds of Rotor 1 and Rotor 3.

In recent literature, some simulation work has been done to study the effects of misalignment in axial flux [28] and radial flux magnetic gears [29]. In [28], the authors found that torque was reduced when the LSR is misaligned translationally. However, only one design was investigated. In this study, as in [29], parametric sweeps were conducted to characterize the axial flux magnetic gear's response to multiple types of static misalignments. Fig. 2 illustrates different static misalignments in an AFMG. Translational and angular static misalignment of Rotor 1 and Rotor 3 are considered and sensitivity to misalignment is evaluated using the change in a gear's torque signature during misalignment relative to that gear's torque profile with zero misalignment. This paper is the first to analyze the effects of misalignment on torque ripple and magnetic forces. As almost 50% of wind turbine gearbox failures are caused by the high-speed shaft bearings [5], [9], understanding the torque ripple and magnetic forces on the high-speed rotor (Rotor 1) will indicate if the AFMG is worthy of further investigation for wind turbine drivetrain applications. This paper is also the first to include results from an experimental prototype to study the effects of static transverse misalignment in an AFMG.

II. Design Study Methodology

To examine the effects of misalignment on a variety of magnetic gear designs, a parametric study was evaluated using 3D finite element analysis (FEA). Each simulation uses NdFeB N42 permanent magnets with a 1.3 T remanence and modulators and back irons made of Somaloy 700 3P, a soft magnetic composite. Three base designs with various gear ratios and the parameters shown in Table I were considered. The derived parameter k is the ratio of the inner radius of the permanent magnets and modulators to their outer radius. As in [26], G_{Int} is the integer part of the gear ratio. To keep torque ripple and off-axis torques relatively low, G_{Int} relates the pole pair counts by

$$P_3 = \begin{cases} G_{Int} \cdot P_1 + 1 & \text{for } (G_{Int} + 1) \cdot P_1 \text{ odd} \\ G_{Int} \cdot P_1 + 2 & \text{for } (G_{Int} + 1) \cdot P_1 \text{ even} \end{cases} \tag{3}$$

For each base design, the parameters in Table II were each swept individually; however, $P_1 = 9$ was only evaluated for $G_{Int} = 2$, so there were a total of 40 design combinations. For each of these combinations, the Rotor 1 and Rotor 3 transverse and angular static misalignment conditions shown in Fig. 2(b) and Fig. 2(c) were swept to determine the sensitivity of each design to misalignment. Each design was simulated at full load to determine the torque ripple, average slip torque, magnetic forces and off-axis torques on each rotor.

TABLE I. Base Design Parameters

Parameter	*Values*	*Units*
Integer part of gear ratio (G_{Int})	2, 5, 8	
Rotor 1 pole pair count (P_1)	5	
Outer radius (R_{Out})	100	mm
Rotor 1 PM thickness (T_{PM1})	12	mm
Rotor 3 PM thickness (T_{PM3})	12	mm
Modulator thickness (T_{Mods})	6	mm
Radii ratio (k)	0.5	
Air gap thickness (T_{AG})	1	mm

TABLE II. Parameters Swept in Each Base Design

Parameter	*Values*	*Units*
Rotor 1 pole pair count (P_1)	3, 5, 7, 9	
Outer radius (R_{Out})	60, 100, 140	mm
Rotor 1 PM thickness (T_{PM1})	6, 12, 18	mm
Rotor 3 PM thickness (T_{PM3})	6, 12, 18	mm
Modulator thickness (T_{Mods})	6, 9, 12	mm
Radii ratio (k)	0.25, 0.5, 0.75	

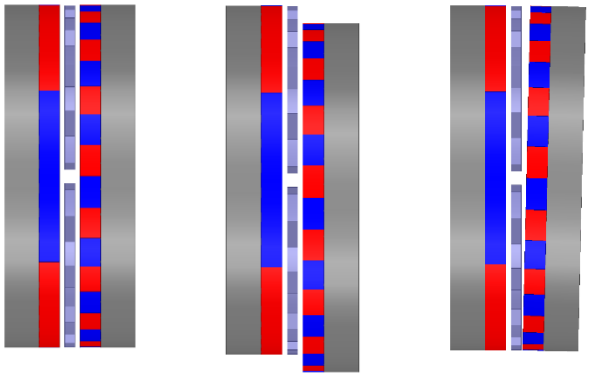

Fig. 2. (a) No misalignment, (b) static transverse Rotor 3 misalignment, and (c) static angular Rotor 3 misalignment scenarios.

III. Simulation Results

A. Transverse Rotor Misalignment

Fig. 3-7, which show effects of misalignment for a particular design case, illustrate that misalignments of Rotor 1 and Rotor 3 impact a gear's operation differently. Fig. 4 demonstrates that transverse misalignment not only lowers the average slip torque but also increases peak-to-peak torque ripple, consequently increasing torque ripple percentage, defined as

$$\text{Torque Ripple (\%)} = \frac{T_{max}-T_{min}}{T_{avg}} \times 100\%, \quad (4)$$

where T_{max}, T_{min}, and T_{avg} are the maximum, minimum, and average torques, respectively. Fig. 5 shows that the net axial force acting on each rotor does not significantly change. It was found that the net axial force did not significantly change for any design considered in this study during transverse misalignment and usually decreased slightly in magnitude under misalignment conditions. It is beneficial that no significant decrease on one side happens, as a reduction of axial forces on one rotor result could result in higher net axial force on the modulators [27]. Fig. 6(a) shows the magnitude of the maximum axial force acting on any individual modulator, and Fig. 6(b) shows the magnitude of the maximum tangential force acting on any individual modulator. Fig. 6 illustrates that no significant change in these forces occurs with transverse misalignment of either rotor.

Fig. 3. Legend for Figs. 4-6.

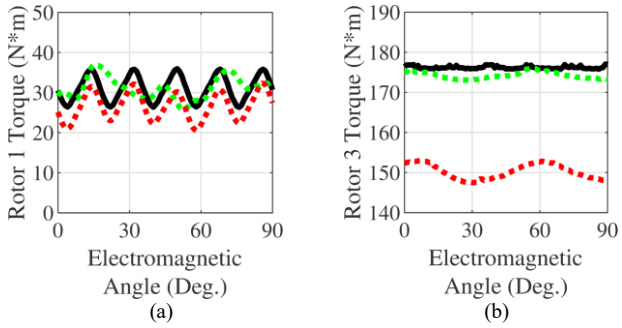

Fig. 4. (a) Rotor 1 and (b) Rotor 3 torque waveforms for continuous operation at the maximum torque orientation of a design with G_{Int} = 5, P_1 = 3, k = 0.5, and R_{Out} = 100 mm under perfect alignment, a 3 mm Rotor 1 transverse misalignment, and a 3 mm Rotor 3 transverse misalignment.

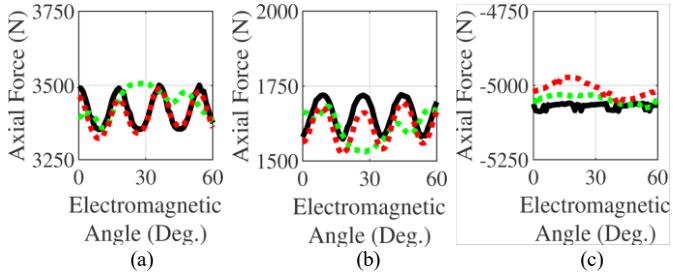

Fig. 5. (a) Rotor 1, (b) Rotor 2 (modulators), and (c) Rotor 3 axial force waveforms for continuous operation of a design with G_{Int} = 5, P_1 = 3, k = 0.5, and R_{Out} = 100 mm at the maximum torque orientation under perfect alignment, a 3 mm Rotor 1 transverse misalignment, and a 3 mm Rotor 3 transverse misalignment.

Because these changes of the forces are negligible from a design point of view, they are not discussed throughout the remainder of this paper. While existing forces do not significantly change, Fig. 7 illustrates that transverse misalignment introduces oscillating off-axis torques on Rotors 1 and 3. Off-axis torques on Rotor 1 are of the greatest concern because of the higher speeds, and the high-speed bearings are where the majority of wind turbine gearbox failures occur [9]. All results in this section are for transverse misalignment along the x-axis in the direction of a slot in Rotor 2. It was found that a design's sensitivity to misalignment was not significantly affected by whether the misalignment was in the direction of a modulator or a slot. Figs. 3-7 serve merely as an example, as the different designs vary in their sensitivity to transverse misalignment. The simulations reveal that the magnet and modulator thicknesses have a negligible effect on an AFMG's sensitivity to transverse misalignment. Alternatively, pole pair counts (P_1 and P_3), the radii ratio (k), and the outer radius (R_{Out}) impact an AFMG's sensitivity to transverse and angular misalignment.

Figs. 8-24 illustrate the impact of Rotor 1 and Rotor 3 transverse misalignment (see Fig. 2(b)) on Rotor 3 slip torque, Rotor 1 torque ripple, and Rotor 1 and 3 off-axis torques. For each design, the Rotor 1 torque ripple percentage values are plotted as defined by (4). Each design's Rotor 3 slip torque is normalized to the Rotor 3 slip torque of the perfectly aligned case for that particular design to illustrate sensitivity to

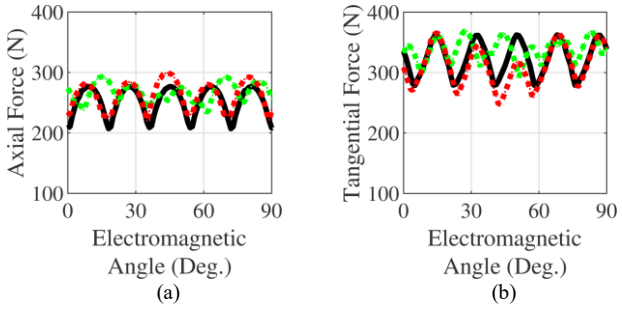

Fig. 6. (a) Maximum axial force magnitude and (b) maximum tangential force magnitude on any individual modulator for continuous operation of a design with G_{Int} = 5, P_1 = 3, k = 0.5, and R_{Out} = 100 mm at the maximum torque orientation under perfect alignment, a 3 mm Rotor 1 transverse misalignment, and a 3 mm Rotor 3 transverse misalignment.

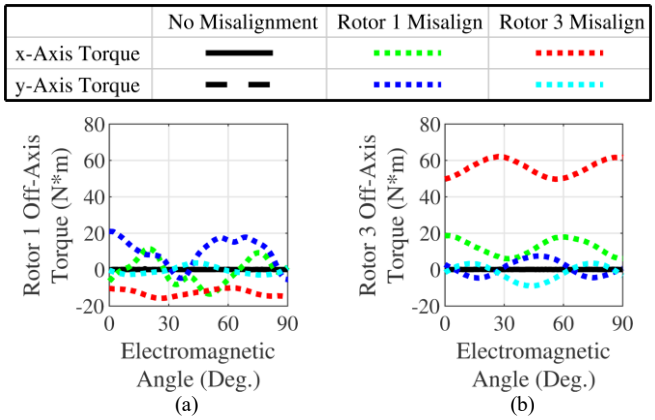

Fig. 7. (a) Rotor 1 and (b) Rotor 3 off-axis torque waveforms for continuous operation of a design with G_{Int} = 5, P_1 = 3, k = 0.5, and R_{Out} = 100 mm at the maximum torque orientation under perfect alignment, a 3 mm Rotor 1 transverse misalignment, and a 3 mm Rotor 3 transverse misalignment.

misalignment as a per unit (p.u.) quantity. Figs. 4, 9, 15, 20, and 21 show that an AFMG's slip torque is much more sensitive to Rotor 3 misalignment than it is to equal Rotor 1 misalignment. This is due to the higher PM pole count on Rotor 3. Figs. 10, 16, and 22 demonstrate that Rotor 1 torque ripple percentage is more sensitive to Rotor 1 misalignment. The Rotor 1 torque ripple is already higher than the Rotor 3 torque ripple because the least common multiple of P_1 and Q_2 is lower than that of P_3 and Q_2, resulting in the larger magnitude and lower fundamental order of the Rotor 1 torque ripple waveform [16]. Rotor 1 torque ripple percentage is more sensitive to Rotor 1 transverse misalignment because the ripple component grows most quickly as Rotor 1 is transversely misaligned. Off-axis torques are generally larger on the transversely misaligned rotor, but Figs. 7, 12-13, 17-18, and 23-24 show that misaligned rotors can transmit off-axis torque to the opposite rotor.

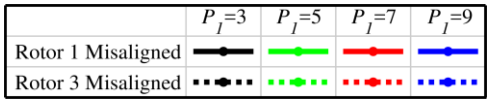

Fig. 8. Legend for Figs. 9-13.

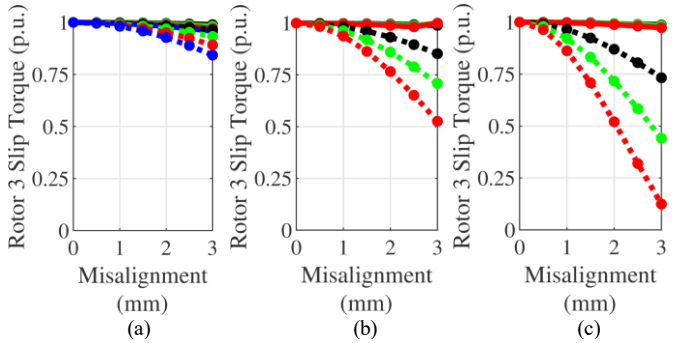

Fig. 9. Variation of normalized Rotor 3 slip torque at different pole pair counts for (a) G_{Int} = 2, (b) G_{Int} = 5, and (c) G_{Int} = 8 with Rotors 1 and 3 misalignment.

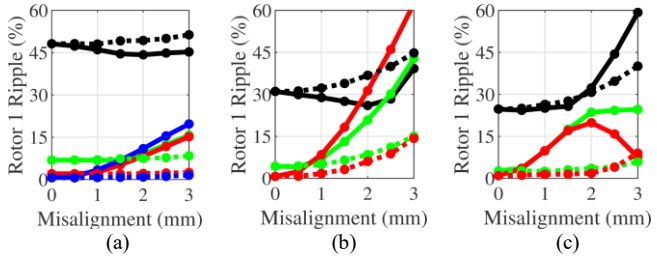

Fig. 10. Variation of Rotor 1 torque ripple percentage at different pole pair counts for (a) G_{Int} = 2, (b) G_{Int} = 5, and (c) G_{Int} = 8 with Rotors 1 and 3 misalignment.

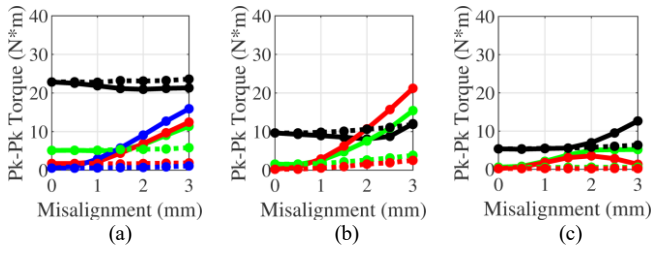

Fig. 11. Variation of Rotor 1 peak-to-peak torque at different pole pair counts for (a) G_{Int} = 2, (b) G_{Int} = 5, and (c) G_{Int} = 8 with Rotor 1 and 3 misalignment.

Fig. 9 demonstrates that increasing P_1 increases the design's sensitivity to misalignment. Similarly, increasing the gear ratio, which increases P_3, also increases the design's sensitivity to misalignment. As P_3 increases, an AFMG's slip torque decreases more rapidly with misalignment. This occurs because increased pole counts produce shorter pole arcs and shorter flux paths, which are more significantly affected by misalignment than longer flux paths. For example, the design with the highest pole count considered in this study experienced a 90% reduction in slip torque at 3 mm (1.5% of the outer diameter) of Rotor 3 misalignment, as indicated in Fig. 9(c). Fig. 10 reveals that the lowest pole count and lowest gear ratio designs yield the highest torque ripple for the perfectly aligned case, which agrees with the observations of previous studies [16]. Fig. 10 also illustrates that increasing P_1 increases the design's sensitivity to misalignment with regard to torque ripple as well, though the driving reason for the ripple increase differs for Rotor 3 and Rotor 1 misalignment. Fig. 11 reveals that the increase in Rotor 1 torque ripple percentage caused by Rotor 3 misalignment is primarily driven by the reduction in slip torque shown in Fig. 9, rather than an increase in the peak-to-peak torque. However, as shown in Figs. 4 and 9, transverse misalignment of Rotor 1 does not significantly reduce the average slip torque. Therefore, the increase in Rotor 1 torque ripple percentages caused by Rotor 1 misalignment is primarily driven by the increase in the magnitude of the ripple component. Interestingly, the Rotor 1 torque ripple of the design with the lowest pole pair count and gear ratio shown in Fig. 10(a) is slightly reduced by Rotor 1 transverse misalignment because misalignment actually reduces the peak-to-peak component, as shown in Fig. 11(a). For designs with high pole counts and gear ratios, Rotor 1 transverse misalignment increases the ripple component quickly, but a local maximum exists as observed in Fig. 11(c). Because the peak-to-peak torque ripple decreases but the average torque does

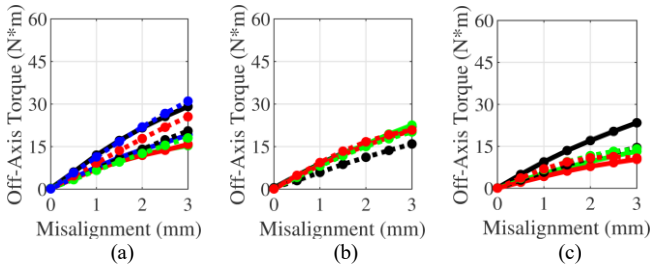

Fig. 12. Variation of off-axis torque magnitude acting on Rotor 1 at different pole pair counts for (a) G_{Int} = 2, (b) G_{Int} = 5, and (c) G_{Int} = 8 with Rotors 1 and 3 misalignment.

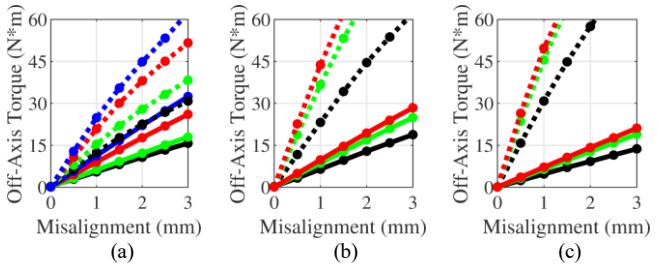

Fig. 13. Variation of off-axis torque magnitude acting on Rotor 3 at different pole pair counts for (a) G_{Int} = 2, (b) G_{Int} = 5, and (c) G_{Int} = 8 with Rotor 1 and 3 misalignment.

not significantly decrease for Rotor 1 misalignment, the Rotor 1 torque ripple appears to decrease for the highest pole count and highest gear ratio designs. Figs. 12-13 demonstrate that increasing P_1 or P_3 generally increases a design's sensitivity to off-axis torques caused by misalignment.

Figs. 14-18 show that the ratio of the inner radius to the outer radius, k, affects an AFMG's sensitivity to misalignment. Fig. 15 shows that the slip torques of designs with low k values suffer more from misalignment. This is because these designs have shorter pole arcs and flux paths near the inner radius. Fig. 16 shows that designs with the largest k values exhibit the highest torque ripple for the perfectly aligned case. The torque ripple percentage increases most quickly for designs with smaller k values because average torque decreases and ripple increases most quickly for these designs. Figs. 17-18 show that designs with larger k values experience smaller off-axis torques for the same misalignment. This is because these designs have smaller air gap surface areas. Thus, Figs. 17-18 reveal that designs with larger k values, or smaller air gap surface areas, are generally more tolerant to misalignment with respect to off-axis torques.

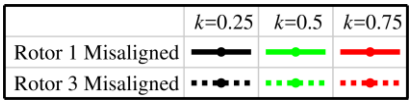

Fig. 14. Legend for Figs. 15-18.

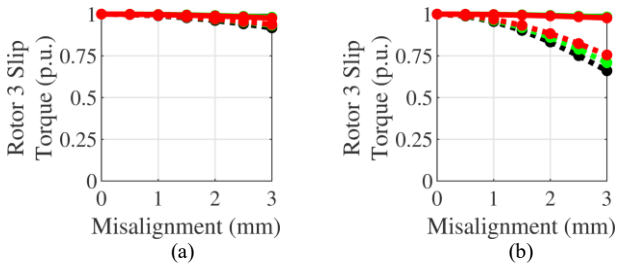

Fig. 15. Variation of normalized Rotor 3 slip torque at different radii ratios for (a) $G_{Int} = 2$ and (b) $G_{Int} = 5$ with Rotors 1 and 3 misalignment.

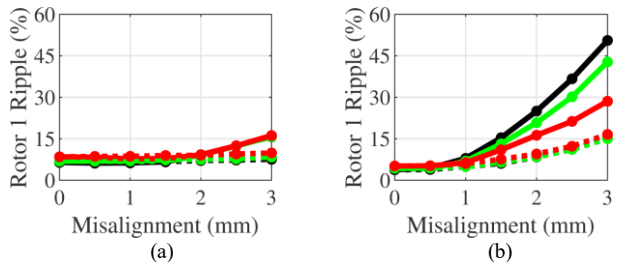

Fig. 16. Variation of Rotor 1 torque ripple percentage at different radii ratios for (a) $G_{Int} = 2$ and (b) $G_{Int} = 5$ with Rotors 1 and 3 misalignment.

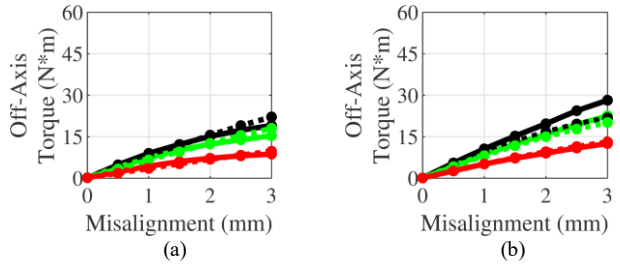

Fig. 17. Variation of off-axis torque magnitude acting on Rotor 1 at different radii ratios for (a) $G_{Int} = 2$ and (b) $G_{Int} = 5$ with Rotor 1 and 3 misalignment.

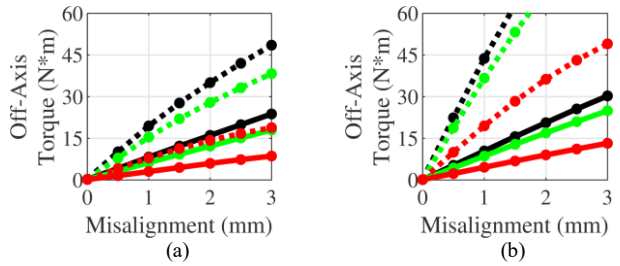

Fig. 18. Variation of off-axis torque magnitude acting on Rotor 3 at different radii ratios for (a) $G_{Int} = 2$ and (b) $G_{Int} = 5$ with Rotor 1 and 3 misalignment.

Figs. 19-24 show that, for a fixed k, the outer radius of an AFMG affects a design's sensitivity to misalignment. Fig. 20 illustrates that an AFMG with a larger radius is more tolerant to the same absolute misalignment. However, in Fig 21, the misalignment is normalized by the outer radius. Fig. 21 reveals that, if the static transverse misalignment is proportional to the AFMG's outer radius, the design's outer radius has little effect on its sensitivity to misalignment. This is useful to keep in mind when considering manufacturing tolerances. Fig. 22 illustrates that the torque ripples exhibited by designs with smaller outer radii are more sensitive to absolute misalignment. Figs. 23-24 show that larger radii designs experience larger off-axis torques for the same absolute misalignment. This is because, for the same k, designs with larger outer radii have larger air gap surface areas. This means that the ratings of the bearings for an AFMG quickly increase as its outer radius increases. Thus, Figs. 19-24 show that larger radii AFMG designs are less sensitive to the same absolute misalignment with regard to torque ripple, but more sensitive with regard to off-axis torques.

B. Angular Rotor Misalignment

Figs. 25-33 illustrate the impacts of angular misalignment. In these graphs, the x-axis is defined as percent air gap closure. For this design study, an air gap of 1 mm was set, and the maximum angular misalignment of 50% corresponds to a design in which the air gap of the given rotor is 0.5 mm one edge, and 1.5 mm on the side opposite. It was found that, within the considered range, angular misalignment never made a significant impact on the average torque, regardless of which rotor was angularly misaligned. It was also observed that Rotor 3 angular misalignment made no significant impact on Rotor 1 or Rotor 3 torque ripple. Rotor 1 torque ripple did change for designs with the lowest pole count considered, but the change was less than 5%. This change was driven primarily by a change in the ripple component magnitude. Both Rotor 1 and Rotor 3 angular misalignment increased axial forces on the misaligned rotor, but the increase was not significant compared to the large axial forces present in the perfectly aligned case. On the other hand, angular misalignment significantly increases the off-axis torque acting on a rotor. Pole pair counts, gear ratio, radii ratio, and outer radii influence the sensitivity of a magnetic gearbox design to off-axis torques caused by angular misalignment.

Figs. 25-27 show that designs with higher pole counts and higher gear ratios are more sensitive to angular misalignment. Figs. 28-30 reveal that the off-axis torque's sensitivity to angular misalignment decreases as k increases. This occurs because increasing k decreases the air gap surface area. Figs. 31-33 show

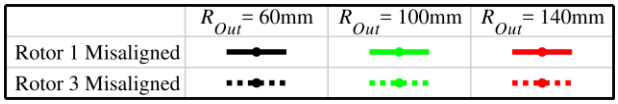

Fig. 19. Legend for Figs. 20-24.

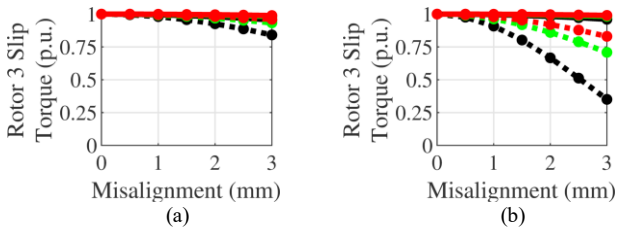

Fig. 20. Variation of normalized Rotor 3 slip torque at different outer radii for (a) G_{Int} = 2 and (b) G_{Int} = 5 with Rotors 1 and 3 misalignment.

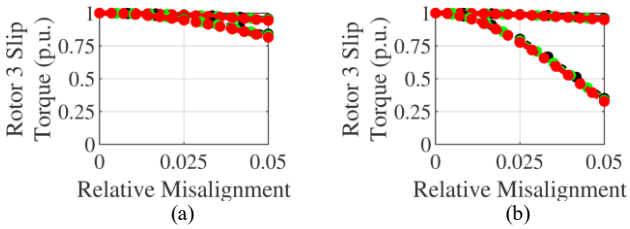

Fig. 21. Variation of normalized Rotor 3 slip torque at different outer radii for (a) G_{Int} = 2 and G_{Int} = 5 by relative (normalized) Rotors 1 and 3 misalignment.

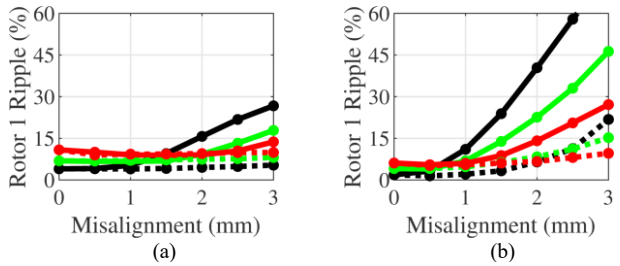

Fig. 22. Variation of Rotor 1 torque ripple percentage at different outer radii for (a) G_{Int} = 2 and (b) G_{Int} = 5 with Rotors 1 and 3 misalignment.

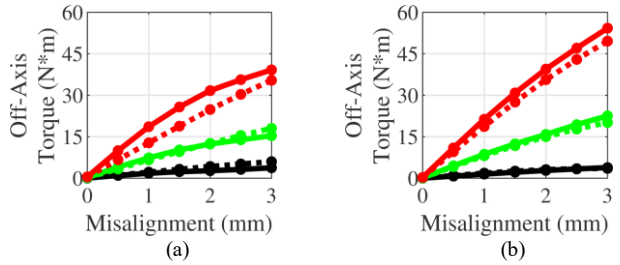

Fig. 23. Variation of off-axis torque magnitude acting on Rotor 1 at different outer radii for (a) G_{Int} = 2 and (b) G_{Int} = 5 with Rotor 1 and 3 misalignment.

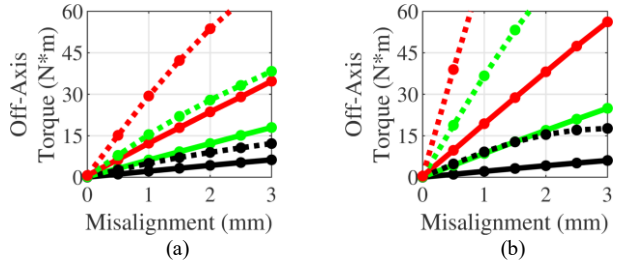

Fig. 24. Variation of off-axis torque magnitude acting on Rotor 3 at different outer radii for (a) G_{Int} = 2 and (b) G_{Int} = 5 with Rotor 1 and 3 misalignment.

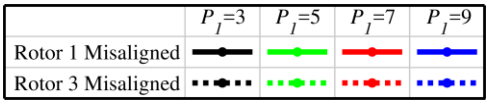

Fig. 25. Legend for Figs. 26-27.

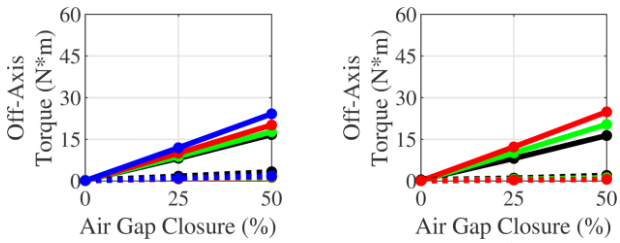

Fig. 26. Variation of off-axis torque magnitude acting on Rotor 1 at different pole pair counts for (a) G_{Int} = 2 and (b) G_{Int} = 5 with Rotor 1 and 3 misalignment.

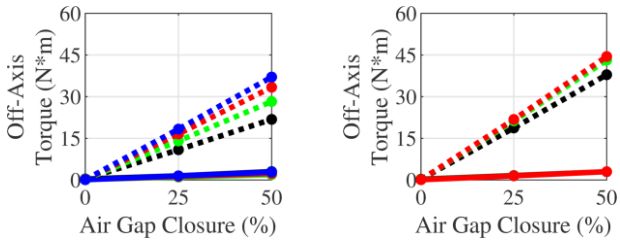

Fig. 27. Variation of off-axis torque magnitude acting on Rotor 3 at different pole pair counts for (a) G_{Int} = 2 and (b) G_{Int} = 5 with Rotor 1 and 3 misalignment.

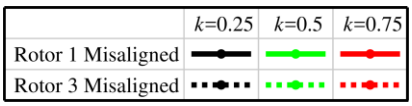

Fig. 28. Legend for Figs. 29-30.

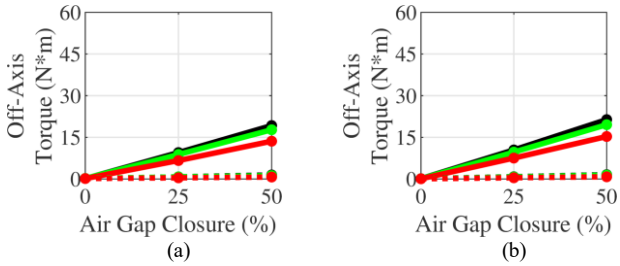

Fig. 29. Variation of off-axis torque magnitude acting on Rotor 1 at different radii ratio for (a) G_{Int} = 2 and (b) G_{Int} = 5 with Rotor 1 and 3 misalignment.

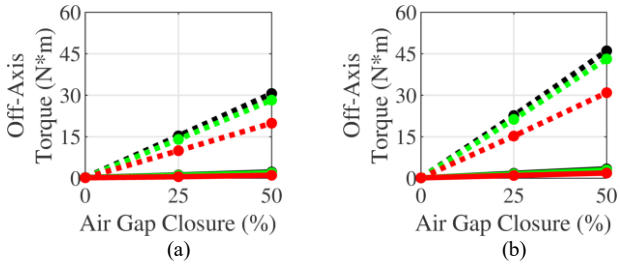

Fig. 30. Variation of off-axis torque magnitude acting on Rotor 3 at different radii ratio for (a) G_{Int} = 2 and (b) G_{Int} = 5 with Rotor 1 and 3 misalignment.

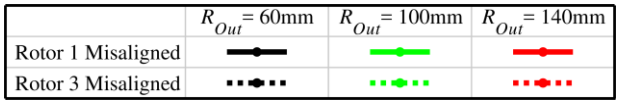

Fig. 31. Legend for Figs. 32-33.

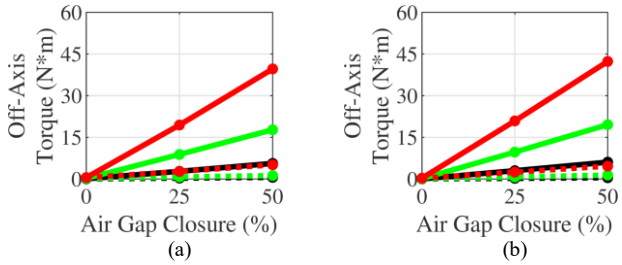

Fig. 32. Variation of off-axis torque magnitude acting on Rotor 1 at different outer radii for (a) G_{Int} = 2 and (b) G_{Int} = 5 with Rotor 1 and 3 misalignment.

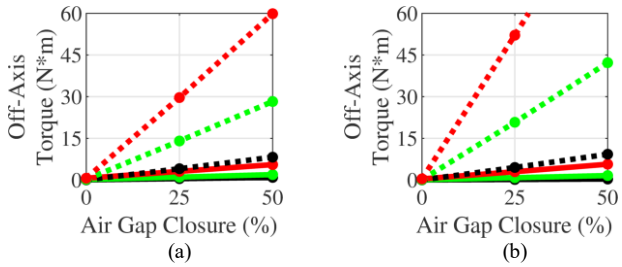

Fig. 33. Variation of off-axis torque magnitude acting on Rotor 3 at different outer radii for (a) G_{Int} = 2 and (b) G_{Int} = 5 with Rotor 1 and 3 misalignment.

that, for a fixed k, designs with larger outer radii experience larger off-axis torques for the same percent air gap closure. This is because designs with larger outer radii have larger air gap surface areas. The thicknesses of the rotor magnets and modulators have negligible effects on the sensitivity of an AFMG to angular misalignment. The difference between the results of angular misalignment towards a modulator or towards a modulator slot was also negligible.

IV. Experimental Results

A prototype AFMG was developed to validate the simulation models. The prototype parameters are detailed in Table III. Additionally, a test setup for varying the Rotor 1 and Rotor 3 transverse misalignments was fabricated. The prototype is shown on the test setup in Fig. 34. Several non-optimal design choices were made in the design of the AFMG to facilitate the development of a prototype and testbed that allow variation of the air gaps and transverse misalignment, while preserving structural integrity and providing access for measurements. The

TABLE III. AFMG Prototype Parameters and Materials

Parameter	*Values*	*Units*
Rotor 1 pole pair count (P_1)	3	
Rotor 3 pole pair count (P_3)	7	
Outer radius (R_{Out})	60	mm
Radii ratio (k)	0.4	
Rotor 1 air gap thickness ($T_{AG,1}$)	7	mm
Rotor 3 air gap thickness ($T_{AG,3}$)	5	mm
Rotor 1 PM thickness (T_{PM1})	12	mm
Rotor 3 PM thickness (T_{PM3})	12	mm
Modulator thickness (T_{Mods})	40	mm
Permanent Magnet Material	N42	
Modulator Material	Somaloy 700 3P	

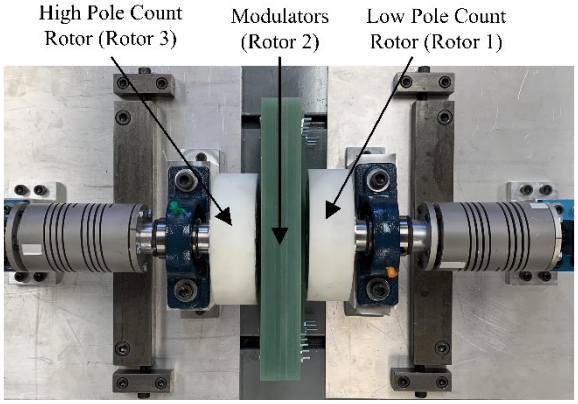

Fig. 34. AFMG prototype on transverse misalignment testbed.

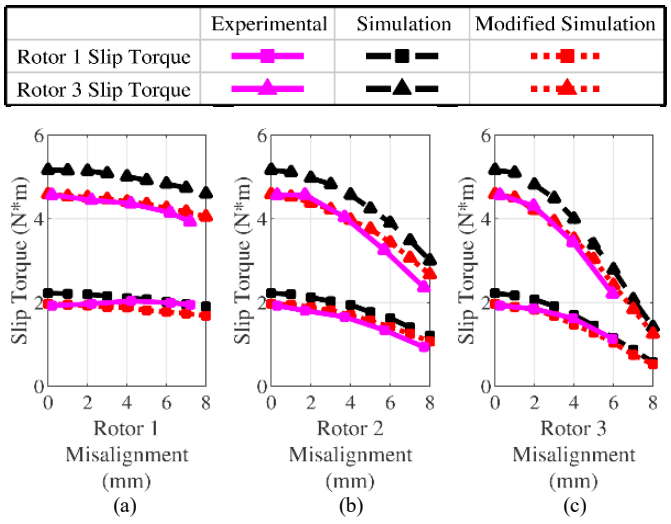

Fig. 35. Rotor 1 and Rotor 3 slip torque of simulated and experimental AFMG with various (a) Rotor 1 misalignment (b) Rotor 3 misalignment and (c) Rotor 2 (modulator ring) misalignment.

rotor magnet sleeves were 3D printed out of inexpensive ABS material. The 40 mm-thick modulator housing was constructed out of garolite (G-10), a nonconductive, nonmagnetic fiberglass-epoxy laminate material with a high Young's modulus, to ensure minimal strain under the high axial stress on the modulators. The air gap was measured in multiple places for each rotor using nonmagnetic feeler gauges, and calipers were used to measure the transverse misalignment. The slip torque was measured at various transverse misalignment conditions. The experimental data and the simulation results are plotted in Fig. 35. Manufacturing tolerances and measurement error make it difficult to ascertain the accuracy of the spatial measurements, and the large torque ripple resulting from the low pole counts may affect the experimentally measured slip torque. Fig. 35 also shows the results of a modified simulation in which the air gaps were increased by just a half of a millimeter to illustrate how air gap uncertainty resulting from the feeler gauge measurements could affect the slip torque. Nevertheless, the experimental data followed a similar trend as the FEA results.

V. Conclusion

This paper uses a parametric FEA simulation study to provide the first thorough analysis of the effects of misalignment

on an AFMG. The slip torque of the AFMG is most sensitive to Rotor 3 transverse misalignment. Rotor 1 transverse and angular misalignment make a negligible impact on slip torque and Rotor 3 torque ripple, but make a significant impact on the Rotor 1 torque ripple. Increasing the pole counts of the gear significantly increases the gear's sensitivity to misalignment. Additionally, increasing the air gap surface area by reducing the inner radius or by increasing the outer radius makes the off-axis torques larger when the design is misaligned. However, the design parameter values that minimize a design's sensitivity to misalignment may not be the same values that maximize the design's slip torque or minimize its torque ripple under nominal or minimally misaligned conditions. Finally, the experimental results for the slip torque of an AFMG prototype on a testbed designed to allow transverse misalignment followed a similar trend as the simulation results.

ACKNOWLEDGMENT

Portions of this research were conducted with the advanced computing resources provided by Texas A&M Performance Research Computing. The authors would like to thank ANSYS for their support of the EMPE lab through the provision of FEA software. The authors would also like to thank the U.S. Army CCDC Army Research Laboratory for supporting this work.

REFERENCES

[1] B. McNiff, W. D. Musial, and R. Errichello, "Variations in Gear Fatigue Life for Different Wind Turbine Braking Strategies," Solar Energy Res. Inst., Golden, CO, USA, Tech. Rep. TP-257-3984, Jun. 1991.

[2] W. Musial, S. Butterfield, and B. McNiff, "Improving wind turbine gearbox reliability," Nat. Renew. Energy Lab., Golden, CO, USA, Tech. Rep. CP-500-41548, May 2007.

[3] J. Puigcorbe and A. de-Beaumont, "Wind turbine gearbox reliability," *Renew. Energy World*, vol. 13, no. 3, 2010.

[4] P. J. Tavner, J. Xiang, and F. Spinato, "Reliability analysis for wind turbines," *Wind Energy*, vol. 10, no. 1, pp. 1–18, Jul. 2006.

[5] S. Sheng, "Wind turbine gearbox reliability database, condition monitoring, and operation and maintenance research update," Nat. Renew. Energy Lab., Golden, CO, USA, Tech. Rep. PR-5000-66028, Feb. 2016.

[6] T. Stehly and P. Beiter "2018 Cost of Wind Energy Review," Nat. Renew. Energy Lab., Golden, CO, USA, Tech. Rep. TP-5000-74598, Dec. 2019.

[7] H. Polinder, F. F. A. Van Der Pijl, G. J. De Vilder, and P. J. Tavner, "Comparison of direct-drive and geared generator concepts for wind turbines," *IEEE Trans. Energy Convers.*, vol. 21, no. 3, pp. 725–733, Sep. 2006.

[8] S. Knight, "The gearbox repair market continues to grow," *Windpower Monthly*, Aug. 2011. [Online]. Available: https://www.windpowermonthly.com/article/1086978/gearbox-repair-market-continues-grow.

[9] U.S. Department of Energy Wind Energy Technologies Office, "Statistics Show Bearing Problems Cause the Majority of Wind Turbine Gearbox Failures," *Office of Energy Efficiency & Renewable Energy*, Sep. 2015. [Online]. Available: https://www.energy.gov/eere/wind/articles/statistics-show-bearing-problems-cause-majority-wind-turbine-gearbox-failures.

[10] R. Orozco, S. Sheng, and C. Phillips, "Diagnostic Models for Wind Turbine Gearbox Components Using SCADA Time Series Data," Nat. Renew. Energy Lab., Golden, CO, USA, Tech. Rep. CP-5000-71166, Jul. 2018.

[11] S. Sheng, "Wind Turbine Drivetrain Condition Monitoring", Nat. Renew. Energy Lab., Golden, CO, USA, Tech. Rep. PR-5000-52908, Oct. 2011.

[12] S. Sheng, "Monitoring of wind turbine gearbox condition through oil and wear debris analysis: a full-scale testing perspective" *Tribol. Trans.*, vol. 59, no.1, pp. 149-162, 2016.

[13] A. Ragheb and M. Ragheb, "Wind turbine gearbox technologies," in *Proc. Int. Nucl. and Renew. Energy Conf.*, 2010, pp. 1-8.

[14] G. K. Atallah and D. Howe, "A novel high-performance magnetic gear," *IEEE Trans. Magn.*, vol. 37, no. 4, pp. 2844–2846, Jul. 2001.

[15] R-J. Wang and S. Gerber, "Magnetically geared wind generator technologies: Opportunities and challenges," *Appl. Energy*, vol. 136, pp. 817–826, 2014.

[16] N. W. Frank and H. A. Toliyat, "Gearing ratios of a magnetic gear for wind turbines," in *Proc. IEEE Int. Elect. Mach. and Drives Conf.*, 2009, pp. 1224–1230.

[17] H. Polinder et al., "Trends in wind turbine generator systems", *IEEE J. Emerg. Sel. Topics Power Electron*.vol. 1, no. 3, pp. 174–185, Sep. 2013.

[18] K. Davey, L. McDonald and T. Hutson, "Axial Flux Cycloidal Magnetic Gears," *IEEE Trans. Magn.*, vol. 50, no. 4, pp. 1-7, April 2014.

[19] A. B. Kjaer, S. Korsgaard, S. S. Nielsen, L. Demsa and P. O. Rasmussen, "Design, Fabrication, Test, and Benchmark of a Magnetically Geared Permanent Magnet Generator for Wind Power Generation," *IEEE Trans. Energy Convers.*, vol. 35, no. 1, pp. 24-32, Mar. 2020.

[20] K. Li et al., "Electromagnetic analysis and experimental testing of a flux focusing wind turbine magnetic gearbox," *IEEE Trans. Energy Convers.*, vol. 34, no. 3, pp. 1512-1521, Sep. 2019.

[21] V. Asnani, J. Scheidler, and T. Tallerico, "Magnetic gearing research at NASA," in *Proc. of AHS Intl. 74th Annual Forum*, 2018, pp. 1-14.

[22] T. V. Frandsen, P. O. Rasmussen, and K. K. Jensen, "Improved motor integrated permanent magnet gear for traction applications," in *Proc. IEEE Energy Convers. Congr. Expo.*, 2012, pp. 3332–3339.

[23] P. Chmelicek, S. D. Calverley, R. S. Dragan, and K. Atallah, "Dual rotor magnetically geared power split device for hybrid electric vehicles," *IEEE Trans. Ind. Appl.*, vol. 55, no. 2, pp. 1484-1494, Mar./Apr. 2019.

[24] M. Johnson, M. C. Gardner, H. A. Toliyat, S. Englebretson, W. Ouyang, and C. Tschida, "Design, construction, and analysis of a large scale inner stator radial flux magnetically geared generator for wave energy conversion," *IEEE Trans. Ind. Appl.*, vol. 54, no. 4, pp. 3305–3314, Jul./Aug. 2018.

[25] S. Mezani, K. Atallah, and D. Howe, "A high performance axial-field magnetic gear," *J. Appl. Phys.*, vol. 99, 2006, Art. no. 08R303.

[26] M. C. Gardner, M. Johnson and H. A. Toliyat, "Comparison of Surface Permanent Magnet Axial and Radial Flux Coaxial Magnetic Gears," *IEEE Trans. Energy Convers.*, vol. 33, no. 4, pp. 2250-2259, Dec. 2018.

[27] M. Johnson, M. C. Gardner and H. A. Toliyat, "Design and Analysis of an Axial Flux Magnetically Geared Generator," *IEEE Trans. Ind. Appl.*, vol. 53, no. 1, pp. 97-105, Jan.-Feb. 2017.

[28] M. F. H. Khatab, Z.-Q. Zhu, H. Li, and Y. Liu, "Influence of static and dynamic rotor/stator misalignments in axial flux magnetically geared machines," *J. Eng.*, vol. 2019, no. 17, pp. 3991–3996, Jan. 2019.

[29] L. A. Percebon, R. Ferraz, and M. V. F. da Luz, "Modelling of a magnetic gear considering rotor eccentricity," in *Proc. IEEE Int. Elect. Mach. and Drives Conf.*, 2011, pp. 1237–1241.